| 1   | The characteristics of biofilms and decays of free chlorine and monochloramine in drinking  |
|-----|---|
| 2   | water distributions systems with corrosion inhibitors   |
| 3   | Conghui Huang <sup>1</sup> , Tim Ginn <sup>2</sup> , Gemma G. Clark <sup>1</sup> , Farzana R. Zaki <sup>3</sup> , Jungeun Won <sup>3,6</sup> , Stephen A. |
| 4   | Boppart <sup>3,5,6,7</sup> , Thanh H. Nguyen <sup>1,4,5,*</sup>   |
| 5   |   |
| 6   | 1. Department of Civil and Environmental Engineering, University of Illinois at Urbana  |
| 7   | Champaign, Urbana, IL   |
| 8   | 2. Department of Civil and Environmental Engineering, Washington State University   |
| 9   | 3. Beckman Institute for Advanced Science and Technology, 405 North Mathews Avenue,   |
| 10  | Urbana, Illinois 61801, USA   |
| 11  | 4. Institute of Genomic Biology, University of Illinois at Urbana-Champaign, Urbana,  |
| 12  | Illinois, 61801, United States  |
| 13  | 5. Carle Illinois College of Medicine, University of Illinois at Urbana-Champaign, 506  |
| 14  | South Mathews Avenue, Urbana, Illinois 61801, USA   |
| 15  | 6. Department of Bioengineering, University of Illinois Urbana Champaign, 1304 West   |
| 16  | Springfield Avenue, Urbana, Illinois 61801, USA   |
| 17  | 7. Department of Electrical and Computer Engineering, University of Illinois Urbana   |
| 18  | Champaign, 306 North Wright Street, Urbana, Illinois 61801, USA   |
| 19  | Keywords: drinking water biofilms, disinfectant decay, pore structure, corrosion inhibitors   |
| 20  |   |
| 2.1 |   |

#### Abstract

22

23

24

25

26

27

28

29

30

31

32

33

34

35

36

37

38

39

40

41

42

43

44

Disinfectant decay by biofilms in distribution networks during stagnation can allow opportunistic pathogens transmission and thus compromise drinking water safety. Applying phosphate-based corrosion inhibitors to the system can exacerbate disinfectant decay by providing nutrients to biofilms growing inside premise plumbings. Here we evaluate the impacts of corrosion inhibitors on biofilms' structural and chemical properties that form in premise plumbing, and the resulting implications for disinfectant decay. Two commonly used phosphate-based (phosphate blends and phosphate) corrosion inhibitors were added separately to simulated drinking water for biofilm development over one to two years. Optical coherence tomography (OCT) imaging showed that the studied biofilms' thickness, porosity, and porous structure did not change after exposure to free chlorine for 24 hrs or monochloramine for 120 hrs. Compared to other biofilms, phosphatebased biofilms had the highest overall porosity due to their many connecting channels. The phosphate-based biofilms consumed free chlorine or monochloramine at a faster rate than other biofilms. Experimental results showed that phosphate-based biofilms consumed more monochloramine after 96 hours of contact than other biofilms. A separate set of experiments involving disinfectant decay with suspended biomass material, together with the OCT results, provided parameters for a simplified quasi-first-order reaction-diffusion model so that predictive modeling of decay in biofilms under stagnation conditions could be attempted without parameter-fitting. The biofilm modeling results provided a close estimate for free chlorine decay while underestimating monochloramine decay. In agreement with the experimental results, the model results indicate that the phosphate-based biofilms led to slightly faster free chlorine consumption and monochloramine consumption than the other biofilms and indicate that diffusion limitation imposed by biofilm pore structure on disinfectant decay is crucial. The study

results suggest that using phosphate-based corrosion inhibitors may lead to a rapid depletion of residual disinfectant during stagnation.

#### 1. Introduction

45

46

47

48

49

50

51

52

53

54

55

56

57

58

59

60

61

62

63

64

65

66

67

Biofilms are ubiquitous in drinking water distribution systems (DWDSs) (Bloetscher et al., 2010). Drinking water aesthetics, such as color, taste, and odor, can deteriorate when biofilm clusters detach into the DWDSs. Corrosion inhibitors, commonly added to decrease lead and copper corrosion products in drinking water, are usually phosphate-based (about 94% of utilities in the United States) and can provide nutrients to microorganisms grown as biofilms inside DWDS and premise plumbing (Kogo et al., 2017), which connected the end points of DWDS and consumers (Arnold et al., 2020). In compliance with the lead and copper rule, 54% of the utilities in the US used corrosion inhibitors (Arnold et al., 2020). Residual disinfectants (free chlorine and monochloramine) are required by USEPA to maintain microbial stability and prevent opportunistic pathogen propagation in the DWDS and premise plumbing (Prest et al., 2016, Rennecker et al., 2001, Wang et al., 2012). However, residual disinfectants can be depleted by organic matter, biofilms, and pipe material in both large- and small-scale distribution systems, further exacerbated by long stagnation and low flow rate devices implemented for water conservation practice in premise plumbing (Buse et al., 2019b, Lautenschlager et al., 2010, Ley et al., 2020, Li et al., 2019, Ling et al., 2018, Tolofari et al., 2021, Wang et al., 2012). Opportunistic pathogens can find shelter in biofilms and increase the infection risk for water users when the disinfectant concentrations are inadequate (Abdel-Nour et al., 2013, Cooper and Hanlon, 2010, Declerck, 2010, Declerck et al., 2009, Farhat et al., 2012). The disinfectant decay depends on multiple factors, including natural organic matter in the water, scaling extent on the pipe surface, and the pipe material in the DWDS (Wang et al., 2013a, Xue and Seo, 2013).

Disinfectant reactivity has been measured with single-cell cultures, suspended particles in drinking water sources, single-species biofilm clusters, and biofilms harvested from simulated drinking water sources (Boccelli et al., 2003, Du et al., 2022, Lee et al., 2011, Zhao et al., 2018). Chlorine decay in large-scale DWDSs has been modeled based on these disinfectant reactivities. At the same time, biofilms were always multi-species and developed under various water sources and hydraulic regimes (Abokifa et al., 2016a, Abokifa et al., 2016b, Douterelo et al., 2016, Fish et al., 2017, Fish et al., 2015, Zhu et al., 2020).

68

69

70

71

72

73

74

75

76

77

78

79

80

81

82

83

84

85

86

87

88

89

90

Kinetics of free chlorine decay is commonly modeled using first-order kinetics, in largescale distribution (e.g., Monteiro et al., 2014) and premise plumbing networks (Zheng et al., 2015), and while chloramine decay is often modeled as first-order kinetic with additional autodecay, more rigorous simulation requires significantly more complex approaches (Hossain et al., 2022). In either case, biofilm presence has been indicated as an additional factor impacting decay kinetics and disinfection progress (e.g., Buse et al., 2019a, Huang et al., 2020a), requiring separate consideration of kinetics associated with the biofilm (Monteiro et al., 2014; Hossein et al., 2022). Extracellular polymeric substance (EPS) composition of biofilms, affected by hydraulic conditions and water constituents in the DWDS, exhibit different relative disinfectant byproduct formation potentials after chlorine exposure (Liu et al., 2017). Water-filled pores and channels in the biofilm matrix have been shown to accommodate the aqueous-phase transport of chemicals, such as nutrients, oxygens, and disinfectants within single-species lab-grown biofilms (Lee et al., 2018, Quan et al., 2022). Previous studies have shown that the penetration of free chlorine into biofilms by diffusion is impacted by its strong oxidant nature that leads to a fast reaction with biofilm material, while monochloramine can penetrate deeper into the biofilm matrix due to its lower reactivity (Lee et al., 2018, Lee et al., 2011). These observations suggest

that biofilm structure may play a significant role in disinfectant transport and effectiveness. However, effective diffusion coefficients of mature biofilms depend on the structural heterogeneity of biofilm, which can be altered by phosphorus addition, a common ingredient in corrosion inhibitors (Davit et al., 2013, Fang et al., 2009, Quan et al., 2022). Thus, the effect of biofilms' structure and chemical composition developed under these common corrosion inhibitors on disinfectant decay should be studied.

To fill the knowledge gaps on the role of corrosion inhibitors on biofilm characteristics and free chlorine and monochloramine consumption by these biofilms in the premise plumbing, we 1) characterized the structure and chemical composition of biofilms fed by three corrosion inhibition conditions using optical coherence tomography (OCT) and Fourier-transform infrared spectroscopy (FTIR); 2) measured the reactivity of two disinfectants with biomass harvested from three biofilms; 3) determined the disinfectant decay after stagnation contact with three intact biofilms, and modeled decay as a reaction-diffusion process within the biofilm; and 4) characterized the pore structure of the three biofilms by pore network analysis. Biofilms developed under unmodified source water (local groundwater) were used as a control. Two corrosion inhibitors, phosphate or phosphate blends, were chosen because of their popularity in utility that preferred corrosion inhibitors (Arnold et al., 2020). These corrosion inhibitors were added separately to the source water to investigate the differences in biofilm development induced by source water chemistry and disinfectant demand.

#### 2. Methods

A schematic of this study is shown in Figure 1.

117

118

119

120

121

122

123

124

125

126

127

128

129

130

131

132

133

134

135

136

115

### 2.1. Biofilm growth conditions

Biofilms were grown on coupon-holding polypropylene (PP) rods and polyvinyl chloride (PVC) coupons, materials commonly found in premise plumbing systems. These rods and coupons were inserted into three separate CDC reactors (BioSurface Technologies Corporation) fed by groundwater with or without corrosion inhibitors. Groundwater, the drinking water source in Champaign, IL, was passed through a green-sand filter to remove precipitate formed by calcium and magnesium when groundwater is exposed to air. The original groundwater did not contain disinfectants. Two chemical compositions were used in this study due to their popularity in utilities: 1) phosphate (2 mg/L as PO<sub>4</sub>) and 2) phosphate blends (2.4 mg/L as PO<sub>4</sub>). Groundwater without corrosion inhibitors was fed to a separate reactor as a control condition. Sodium diphosphate (Fisher) was mixed with 10L groundwater at a final concentration of 2 mg/L as PO<sub>4</sub> to feed phosphate biofilm. Groundwater containing phosphate blends was prepared by mixing sodium diphosphate (Fisher) and sodium metaphosphate (Fisher) in a 6:4 molar ratio with 10L groundwater at a final concentration of 2.4 mg/L as PO<sub>4</sub>. These concentrations of corrosion inhibitors are in the range of reported corrosion inhibitors used in the US (McNeill and Edwards, 2002, USEPA, 2016). These feeding groundwater solutions were prepared every two days and fed to the CDC reactors continuously at a flow rate of 1.3 mL/min. A stirrer in the CDC reactor created a shear condition with a Reynolds number around 3570. The CDC reactors were wrapped with aluminum foil and kept at an average temperature of 25 °C. The biofilms were grown for over one year before being used in the free chlorine experiments. Although the

biofilms were grown for over two years before being used in the monochloramine experiments, these biofilms had similar chemical and porous characteristics (See results and **Table 1S**).

## 2.2. Biofilm porous structure characterization

Structures of the three studied biofilms were characterized by cross-sectional scans with a dimension of 3.125 mm × 4.18 mm × 4 mm using optical coherence tomography (OCT). The axial resolution of the OCT was around 8 µm, and the lateral resolution was around 20 µm. Three locations were chosen randomly from each biofilm-covered coupon. The OCT images were rotated to correct for taking images at an angle and modified to reduce reflection caused by water using ImageJ Fiji v 2.0 (Schindelin et al., 2012) and Avizo (Thermo Fisher Scientific). About 100-180 images from each image stack were selected for analysis because of the image quality, as described in a previous study (Huang et al., 2020b). The overall biofilm thickness was determined using a MATLAB code described previously (Derlon et al., 2012, Shen et al., 2015). The physical thickness of biofilm was determined by dividing the optical thickness by the corresponding refractive index from 1.33-1.38. The average thickness of each biofilm image stack was calculated as described in previous studies (Huang et al., 2020b).

The upper and lower half of the biofilm OCT image stacks were analyzed separately after dividing the biofilm at half of the average thickness. The porosities and pore network were characterized in the top and bottom halves of the biofilms using the image analysis framework described in a previous study (Huang et al., 2020b).

### 2.3. Chemical composition characterization by FTIR

We used FTIR experiments to determine the biofilm composition. Biomass was scraped from the holding rods into clean petri dishes and dried overnight at 4 °C. Two biomass samples were subjected to FTIR scans, in which 15 scans were obtained for each biofilm type. The

absorbance of the infrared radiation by the dried biomass over the wavenumber from 400 to 4000 cm<sup>-1</sup> was measured by Fourier-transform infrared spectroscopy equipped with an attenuated total reflection element (ATR-FTIR). The wavenumbers associated with the absorbance peaks were compared to the IR spectrums reported in previous studies (Holman et al., 2009, Schmitt and Flemming, 1998).

166167

168

169

170

171

172

173

174

175

176

177

178

179

180

181

182

183

184

161

162

163

164

165

## 2.4. Disinfectant decay in contact with suspended biomass

Our first decay experiments involve reactions with biomass scraped from the coupon biofilm and sonicated to form a suspension. A free chlorine (2 g/L as Cl<sub>2</sub>) stock solution was prepared by diluting sodium hypochlorite (10-15% available chlorine, Sigma) with Milli-Q water. A monochloramine stock solution (510 mg/L as Cl<sub>2</sub>) was prepared by mixing the ammonium chloride solution (1000 mg/L as NH<sub>3</sub>) and sodium hypochlorite to reach an N:Cl molar ratio of 1:1. The stock concentration of free chlorine and monochloramine was determined by measuring the absorbance of the stock at 254 nm and 243 nm (free chlorine and monochloramine, respectively) using a Shimadzu UV-2450 spectrophotometer. The predominance of monochloramine was confirmed by the presence of the only absorbance peak at 243 nm in an absorbance scan made from 190 to 500 nm. The free chlorine and chloramine stock were stored in the dark at 4 °C. A 2 mM carbonate buffer (pH: 7.8-8.1) was prepared by dissolving sodium bicarbonate (Fisher Scientific) in Milli-Q water to simulate the drinking water alkalinity condition (200 mg/L as CaCO<sub>3</sub>). A standard curve from 0.02 to 4.2 mg/L as Cl<sub>2</sub> was constructed based on the linear relationship of UV absorbance at the corresponding wavelength and disinfectant concentrations using the DPD standard method. Two points in the standard curve (0.5 and 2 mg/L as Cl<sub>2</sub>) were checked daily, and the error rate was under 5%. The standard curves for free chlorine and chloramine were measured weekly or in cases where the error rate

was over 5%. Fresh stock solutions of free chlorine and monochloramine were prepared weekly. All glassware was washed thoroughly with water treated by a Milli-Q Water Purification system and baked at 550 °C for 2 hours.

Biomass was scraped from the rods in the CDC reactors using a sterilized spatula and dispensed in 50 mL glass vials containing 15 mL bicarbonate buffer. Then, these biofilms were disrupted by 1 min of vortex followed by 20 min of sonication. Free chlorine or monochloramine stock was added to the suspended biomass to reach a final concentration of 4.0-4.1 mg/L as Cl<sub>2</sub>. The vials were wrapped in foil and placed in a shaker for a designated reaction time, after which a 2.5 mL aliquot was filtered through a 0.22 µm PES syringe filter (Millipore), and the free chlorine or chloramine concentration was measured using the DPD standard method. The reaction times were 5, 15, 30, 150 min for free chlorine and 3, 6, 12, 24, and 48 hours for monochloramine. These reaction times were selected based on the reaction time for free chlorine or monochloramine to reach the detection limit of 0.02 mg/L as Cl<sub>2</sub> with biomass in preliminary experiments. To the remaining suspended biomass in buffer, 2.7 g/L sodium thiosulfate was added to quench the residual disinfectant, and then 10N NaOH at a final concentration of 0.25 M (pH at 11) was added to digest the sample. The sample was then placed on a shaker table at 250 rpm for 3 hours in the dark. The volume of sodium thiosulfate needed to neutralize the residual disinfectants was checked with preliminary experiments. These samples were filtered through a 0.22 µm PES filter and the pH was lowered to 2 by adding concentrated HCl. The total organic matter (TOC) concentrations of digested samples were determined by a Shimadzu TOC-VCPH analyzer. Experiments were conducted in triplicates in free chlorine experiments and duplicates in monochloramine experiments because of sample limitation.

207208

185

186

187

188

189

190

191

192

193

194

195

196

197

198

199

200

201

202

203

204

205

206

#### 2.5. Disinfectant decay in contact with intact biofilms

Two biofilm-covered PP rods with three PVC coupons were removed from the CDC reactor and immersed in glass flasks filled with 250 mL bicarbonate buffer. Freshly prepared disinfectant stock (free chlorine or chloramine) was added into the bicarbonate buffer to reach a final concentration of 4 mg/L as Cl<sub>2</sub>. The disinfectant concentration was measured using the DPD method and the corresponding standard curves, as described in section 2.4. As aforementioned sample collection, disinfectant concentrations after the corresponding contact time were measured in a 2.5 mL sample filtered by a 0.22 µm PES syringe filter (Millipore). The remaining samples were quenched with 2.7 g/L sodium thiosulfate. The contact times for biofilms with free chlorine were 1, 3, 6, 12, and 24 hours, and the contact times with chloramine were 3, 6, 12, 24, 48, 72, 96, and 120 hours due to the low reactivity of chloramine. After these times, the biofilms were scraped from the PVC coupons on the rods and resuspended into a 15 mL bicarbonate buffer. As described above, the biofilms were disrupted by vortex and sonication, followed by digestion with NaOH addition in the shaker. TOC concentrations were determined from the digested samples. The mass of biofilms exposed to the disinfectant was estimated by multiplying the TOC concentration after normalized by the scraped area with the biofilm-covered area on the rods.

225

226

227

228

229

209

210

211

212

213

214

215

216

217

218

219

220

221

222

223

224

2.6 Mathematical modeling of reaction with biomass and diffusion-reaction with biofilm

Disinfectant decay in the presence of suspended biomass.

Under conditions of suspended biomass reactant in suspension, we ignore diffusion limitations and treat the time-dependent consumption of free chlorine or chloramine as a quasi-first-order

230 kinetic,

231 [1] 
$$C(t) = C(0)exp(-\lambda_0 Bt)$$

- where C(t) (mg L<sup>-1</sup> as Cl<sub>2</sub>) is the concentration of disinfectant at time t,  $\lambda_0$  (L mg<sub>Biomass</sub><sup>-1</sup> min<sup>-1</sup>)
- 233 is the specific disinfectant decay rate per unit B (TOC) concentration, B (mg L<sup>-1</sup>) is the initial
- biomass concentration measured as TOC. Because we assumed the biomass concentration as a
- constant, Equation [1] is applied as a first-order kinetic.
- 236 Disinfectant diffusion and decay within intact biofilms.
- To simultaneously quantify the time-dependent impacts of both disinfectant diffusion within and
- reaction with porous biofilm, we applied a conventional transient reaction-diffusion model,

239 [2] 
$$\frac{\partial C}{\partial t} = D \frac{\partial^2 C}{\partial x^2} - \lambda_o BC \qquad 0 < t, \qquad 0 < x \le l$$

with initial and boundary conditions

241 [3] 
$$C(x, t = 0) = 0$$
  $t = 0, 0 < x \le l$ 

242 [4] 
$$C(x = 0, t) = C_b(t)$$
  $t \ge 0, x = 0,$ 

- respectively. This model treats the biofilm as a porous slab of finite thickness admitting one-
- 244 dimensional Fickian diffusion of disinfectant concentration C. The biofilm has thickness l, total
- areal extent A, porosity n, diffusion coefficient  $D = nD_b/\tau$  where  $D_b$  is the diffusion coefficient
- of the disinfectant solute in bulk solution, and  $\tau$  is the tortuosity of the biofilm (assumed unity
- per Melo, 2005). The right-hand side of Equation [2] includes the reaction term for disinfectant
- 248 decay.
- At the surface of the biofilm x = 0, the solution in the biofilm is in contact with the bulk solution
- 250 that has a concentration,  $C_h(t)$ . The disinfectant concentration in the bulk solution  $C_h(t)$
- 251 undergoes dynamics due to diffusive ingress of disinfectant into the biofilm at the surface of the
- 252 biofilm (at x = 0) and is governed by

253 [5] 
$$\forall_b \frac{dC_b}{dt} = -AD \frac{\partial C}{\partial x} \qquad t > 0, x = 0$$

with initial condition

255 [6] 
$$C_b(t=0) = C_{bo}$$
  $t=0$ 

Equations [2-6] were solved numerically using a conventional explicit-in-time finite-difference scheme with central differencing used for the diffusion term. This approach is simple to implement but requires honoring the von Neumann condition for stability of the diffusive flux calculation that is implemented here as

$$\Delta t = \frac{\Delta x^2}{6D}.$$

262 Application of the mathematical models.

Predictive modeling requires independent determination of parameters. To determine values of the specific decay rate constant  $\lambda_o$  independently from the biofilm disinfectant decay experiments, we applied Equation [1] to disinfectant concentration decay data obtained from the suspended biomass experiments. For each combination of disinfectant and biomass type, the value of  $\lambda_o B$  in Equation [1] was manually fitted to the disinfectant concentration data from the suspended biomass decay experiments. This fitting was done by minimizing errors between simulated and average (over replicates) decay data over time. The resulting value of  $\lambda_o B$  was then divided by the measured TOC value (B) for these solutions to obtain the specific reaction rate coefficient  $\lambda_o$ . The remaining parameters needed for Equations [2-6] were directly measured and include biofilm area, thickness (mean values from **Figure 3a**), and porosity (mean values from **Figure 3b**). The bulk diffusion coefficient values are taken from standards literature [ $D_b = 8.28 \times 10^{-4}$  cm<sup>2</sup>/min for free chlorine (Tang and Sandall, 1985);  $D_b = 9.96 \times 10^{-4}$  cm<sup>2</sup>/min for monochloramine (Chen et al., 1993)]. The TOC concentration (B) for the intact biofilms was measured separately. For free chlorine cases, this procedure was repeated for all three biofilm

types and completed the independent determination of values of parameters needed for the use of Equations [2-6] to simulate the decay data in the intact biofilm cases. The reaction rate in the case of monochloramine includes auto-decay at first-order, in addition to the kinetic model described above. The auto-decay rate is assumed strictly first-order and determined from concentration decay observed in the abiotic controls, yielding a rate coefficient  $2.0 \times 10^{-5}$  min<sup>-1</sup>. After these adjustments, the same procedure as described above is used to parameterize the overall reaction rate for the monochloramine decay in the biofilms. Speciation reactions endured by monochloramine are not needed because we measured total monochloramine in the decay experiments.

Parameter values obtained are reported in **Table 1**. Also shown are dimensionless Damköhler numbers (" $Da^{II}$ ") for each case, developed as follows. The dimensionless Damköhler number for reaction-diffusion per unit area in a biofilm is the characteristic diffusion time for penetration of the full depth l of the biofilm,  $l^2/4D$ , divided by the characteristic reaction time,  $1/\lambda_0 B_{biofilm}$ . Thus  $Da^{II} = l^2 \lambda_0 B_{biofilm}/nD_b$ , where we have used the fact that  $D = nD_b$  assuming unit tortuosity. Note that this definition of the Damköhler number ignores the contribution of auto-decay occurring with the monochloramine cases, which was at least three orders of magnitude smaller than the biomass-induced decay rate coefficient.

Table 1 is inserted here.

## 2.6. Statistical analysis

Basic statistical analysis on the measurements and simulations of disinfectant residual concentrations in contact with suspended biomass or biofilms at each sampling time and overall biofilm structure (thickness, overall porosities, and normalized pore and throat number) were

carried out by R version 4.2.0. A parametric hypothesis test (Student's t-test) was used when the assumptions of normality and equal variance were met. A nonparametric hypothesis test (Kolmogorov-Smirnov test, or KS test) was used instead when these assumptions were not met. The goodness-of-fit of the model was determined by testing the differences between the simulations and measurements with a two-sided hypothesis test. A significant difference was determined when the p-value was below 0.05.

#### 3. Results and Discussion

### 3.1. FTIR characterization for biofilm composition

The infrared spectra of two-year biofilms are shown in **Figure 2**. The characterization of FTIR spectra for one-year and two-year biofilms is shown in **Table 1S**. Two distinctive IR spectra were obtained for biofilms fed by groundwater with or without phosphate addition. Three major absorbance peaks at around 713, 872, and 1400 cm<sup>-1</sup> were observed in groundwater biofilms but not in biofilms fed by phosphate-based corrosion inhibitors. Absorbance peaks at 713 and 872 cm<sup>-1</sup> represent aragonite or calcite and likely precipitated from groundwater. The presence of these two peaks suggested precipitation of aragonite and calcite in the biofilms fed by groundwater without polyphosphate addition. Similar results have been reported previously (Shen et al., 2018). Absorbance peaks at 1028-1030 cm<sup>-1</sup> were observed in biofilms grown in groundwater with phosphate blends and phosphate but not in groundwater biofilms. Specifically, the absorbances at around 713 and 872 cm<sup>-1</sup> (carbonate species) were three and seven times greater than the absorbance at around 1028 cm<sup>-1</sup> (phosphate species) in groundwater biofilms. However, no peak was found around 713 cm<sup>-1</sup> in phosphate blends and phosphate biofilms.

blends biofilms were expected because phosphate was used as an antiscalant additive to reduce the precipitation of divalent ions in water-filled equipment, such as reverse osmosis membrane systems and heat exchangers. Biofilms grown with and without phosphate also led to a different IR spectrum in organics species. Specifically, major absorbance bands were observed near 1640 cm<sup>-1</sup> and 1547 cm<sup>-1</sup> in biofilms developed with phosphate and phosphate blends but not in groundwater biofilms. These bands were previously reported in proteins (Pousti et al., 2018, Quilès et al., 2010). While no absorbance peak near 2920 and 2850 cm<sup>-1</sup> (lipids) (Pousti et al., 2018) was found in groudwater biofilms, minor absorbance peaks were observed near 2920 and 2850 cm<sup>-1</sup> in phosphate and phosphate blends biofilms. These differences in the IR spectrums in phosphate-based and groundwater biofilms suggested that using corrosion inhibitors containing phosphate can influence the organic species in the biofilm matrix.

In summary, the choice of using phosphate-containing corrosion inhibitors in drinking water resulted in two distinct FTIR spectra. The chemical composition of the biofilm, especially EPS, can affect biofilm formation and stability in drinking water system (Tugarova et al., 2017). Growing conditions, such as water characteristics, microbial structure, and growth period, can shift the chemical composition of the biofilms by biochemical activities (Holman et al., 2009, Pousti et al., 2018, Quilès et al., 2010, Tugarova et al., 2017). Inorganic precipitation was observed in biofilms grown under the influence of elevated divalent cations, which is commonly found in groundwater (Goode and Allen, 2011, Shen et al., 2018). Also, absorbance peaks associated with organic species, such as protein and lipids, were found in phosphate and phosphate blends biofilms but not in groundwater biofilms.

Figure 2 is inserted here.

3.2. Biofilm thicknesses, porosities, and their variation with treatments

First, we compared the thickness for one- and two-year biofilms (**Figure 3**). Among the three one-year biofilms, the groundwater biofilms were the thinnest (median:  $102 \mu m$ , 95% confidence interval (CI): 87 to  $126 \mu m$ ). However, among the two-year biofilms, groundwater biofilms were thickest (median:  $262 \mu m$ , 95% CI: 212 to  $324 \mu m$ ). Alternatively, for a given biofilm type developed with phosphate corrosion inhibitors, one- and two-year biofilms have similar thicknesses (KS test, p > 0.05). The second thickest biofilms were phosphate biofilms  $218 \mu m$  (95% CI: 191 to  $328 \mu m$ , one year) or  $240 \mu m$  (95% CI: 170 to  $335 \mu m$ , two year). Phosphate blend biofilms were the third thickest with a median of  $147 \mu m$  (95% CI: 84 to  $246 \mu m$ , one-year) and  $165 \mu m$  (112 to  $239 \mu m$ , two-year), (KS test, p < 0.05). We found similar and slightly increased thicknesses for biofilms grown with phosphate and phosphate blends for one and two years. The thickness of biofilms grown without corrosion inhibitors more than doubled during the second year. This observation suggests that phosphate allowed the biofilms to grow to a steady-state faster. Thus, the time required for biofilm growth to reach steady state may depend on biofilm age, feed water constituent, and hydrodynamic condition.

After one year of development (**Figure 3b**), the overall porosities of phosphate blends  $(0.28 \pm 0.06)$  were the greatest, followed by those of phosphate biofilms  $(0.24 \pm 0.08)$  and groundwater biofilms  $(0.11 \pm 0.07)$  (KS test, p < 0.05). After two years of development (**Figure 3d**), the average overall porosity of phosphate blends, phosphate, and groundwater biofilms was  $0.30 (\pm 0.06)$ ,  $0.26 (\pm 0.07)$ , and  $0.15 (\pm 0.04)$ , respectively. No significant change in the overall porosities between one- and two-year growth were observed in any of the biofilms (p > 0.05). The overall porosities in biofilms fed by phosphate and phosphate blends were similar (p > 0.05) and significantly greater groundwater biofilms (p < 0.05, KS test).

For the one-year biofilms (Figure 3a), after 24 hours of free chlorine exposure, the average thickness of phosphate biofilm reduced slightly (KS test, p < 0.05), while the average thickness of phosphate blends and groundwater biofilms increased. A similar trend was observed in two-year-old biofilms exposed to monochloramine. This observation showed that short-term exposure to free chlorine and monochloramine did not remove the biofilm. By comparing the upper and lower halves of the biofilm porosities separately (Figure 1S), no significant difference was found in the top or bottom section of phosphate blends biofilm after free chlorine exposure (t test, p > 0.05). The porosities in the bottom section of the phosphate biofilms were reduced after free chlorine exposure (t test, p < 0.05), while the porosities in the top section remained the same (t test, p > 0.05). However, the porosities in either top or bottom section of groundwater biofilms increased after free chlorine exposure (t test, p < 0.05). Similar trends of increasing porosities in the bottom or top section of groundwater biofilms were observed after monochloramine exposure (t test, p < 0.05). In either the top or bottom section of the two-year-old biofilms, groundwater biofilms were the least porous than phosphate-based biofilms before and after monochloramine exposure (t test, p < 0.05). No significant difference in porosities was found in two-year old biofilms between the two sections (p > 0.05). We expected deeper diffusive transport into the biofilm compared to that of free chlorine because of monochloramine's slower reactivity. The porous top and bottom section in the two-year-old phosphate and phosphate blends biofilms may allow the slowly reacting monochloramine transport further into the biofilm matrix. We tested this hypothesis with experimental results presented below.

371

372

373

374

375

376

377

378

379

380

381

382

383

384

385

386

387

388

389

**Figure 3** is inserted here.

393

394

395

396

397

398

399

400

401

402

403

404

405

406

407

408

409

410

411

412

413

392

## 3.3 More connecting pores and throats were found in biofilms grown with phosphate-based corrosion inhibitors

Because the axial resolution of OCT was around 8 µm, we only include the pores and throats with an equivalent radius above 5 µm in our statistical analysis. The numbers of pores and throats in each biofilm used in the free chlorine and monochloramine scenarios were normalized by the total biofilm volume including biomass and pore space. The pore network analysis showed that phosphate blends and phosphate biofilms had more pores per biofilm volume and more connecting throats per biofilm volume than groundwater biofilms (KS test, p < 0.05) (Figure 4A). After one-year growth (Figure 4A), the highest normalized number of pores was found in phosphate and phosphate blends biofilms, followed by groundwater biofilms (KS test, p < 0.05 each). Groundwater biofilms had the lowest normalized number of throats (KS test, p < 0.05 each), while the other two biofilms had a similar number of throats after normalization (KS test, p > 0.05 each). The median normalized number of connecting throats in groundwater biofilms was 20 and 18 times less than that in phosphate blends and phosphate biofilms, respectively. Among the two-year-old biofilms (Figure 4B), phosphate blends and phosphate biofilms had more normalized throats than groundwater biofilms (KS test, p < 0.05). However, no significant difference between the normalized number of pores was found in phosphate, phosphate blends, and groundwater biofilms. Overall, the great abundance of connecting throats in phosphate and phosphate blends biofilms contributed to the greater bulk porosity of these biofilms compared to groundwater biofilms.

Figure 4 is inserted here.

The biofilm structure can be influenced by microbial structure, influent water characteristics, and hydrodynamic conditions (Liu et al., 2016). In this study, biofilms developed under the influence of phosphate-based corrosion inhibitors were more porous with more connecting channels than those developed without phosphate corrosion inhibitors. A similar observation was reported from biofilms developed in groundwater with or without polyphosphate additives (Shen et al., 2018). Previous studies showed that the addition of phosphate induced changes in the microbial community and EPS production (Liu et al., 2016). These changes can play an important role in the reactivity of biofilms with chlorine and monochloramine and the disinfectant byproducts formation (Lemus Pérez and Rodríguez Susa, 2017, Wang et al., 2013b). In the present study, larger connecting channels and pores in the pore structure found in biofilms developed under phosphate-based corrosion inhibitors may aid in the mass transport process of chlorine and chloramine into the biofilm matrix. A similar observation was reported as greater biofilm removal by chlorine and monochloramine was found after phosphorus addition (Fang et al., 2010).

# 3.4 Experimental results: fastest free chlorine and chloramine decay was observed in phosphate-based biofilms

The experimentally determined free chlorine or monochloramine decays were normalized by the biomass TOC concentrations (**Figure 5**). Free chlorine was rapidly consumed by the three types of biomasses within 2 hours of contact. Among the three biomass, the groundwater biomass consumed free chlorine the least, regardless of sampling time (p < 0.05). On the other hand, phosphate-based biomass consumed the most free chlorine at all sampling times (p < 0.05).

However, we did not observe one type of biomass consistently consuming more monochloramine than other types. No significant differences between the TOC-normalized monochloramine concentrations were found within three biomass after 3 and 24 hours of contact (p > 0.05). Groundwater biomass consumed the least monochloramine after 12 hours of contact (p < 0.05).

To determine the effect of the biofilm structure on the disinfectant reactive transport into the biofilms, we exposed the intact biofilms to either free chlorine or monochloramine. The disinfectant decays obtained with three biofilms are shown in Figure 6a and b. Free chlorine was continuously and completely consumed by all three biofilms within 24 hours of reaction, significantly faster than a scenario without biofilm (p < 0.05). In the first hour of contact, no significant difference in free chlorine decay was found among the three biofilms. After 3 hours of contact, the phosphate biofilms consumed the most free chlorine, while the groundwater biofilms consumed the least free chlorine among the three biofilms (p < 0.05). In the first three hours of contact, the three biofilms consumed monochloramine at a similar rate (p > 0.05). Monochloramine was consumed after 96 hours of contact with biofilms grown with phosphatebased additives. However, after about 60% of monochloramine was consumed by the groundwater biofilms, monochloramine decay continued at a much slower rate (after 96 hours). This reduced consumption of monochloramine may be due to the presence of fewer connecting throats and reduced porosities in top in the groundwater biofilms because these throats may promote the transport of monochloramine into the biofilm matrix and lead to complete consumption in phosphate-based biofilms.

460

461

439

440

441

442

443

444

445

446

447

448

449

450

451

452

453

454

455

456

457

458

459

**Figure 5** is inserted here.

# 3.5 Theoretical framework can simulate free chlorine decay with biofilms but cannot simulate monochloramine decay

We first determined the specific reaction rate constants  $(\lambda_0)$  per biomass type exposed to either free chlorine or monochloramine to answer the question of whether the water chemistry under which the biomass developed impacts the disinfectant reactivity with the biomass. The pseudo-first-order reaction kinetics (Equation [1]) was used to model the disinfectant concentration as a function of time for free chlorine or chloramine in contact with the suspended biomass obtained from three biofilms, respectively. Measured vs. predicted disinfectant concentrations in biomass suspensions are plotted in Figure 2S. The differences between simulated and measured free chlorine concentrations were significant with three biomass cases at most sampling times (t test, p < 0.05). The only exception was with groundwater and phosphate biomass after 15 and 120 min of reaction with free chlorine. However, no significant differences were observed between simulated and measured monochloramine concentrations with all three suspended biomass after 12 hours of reaction with monochloramine (t test, p > 0.05). Slightly greater average monochloramine concentrations were simulated than measurements with phosphate blends and groundwater biomass after three hours of reaction and two phosphatecontaining biomass after six hours of reaction (t test, p < 0.05). As shown in **Table 1**, the free chlorine rate constants were the greatest with biomass grown without corrosion inhibitors compared to those grown with phosphate-based corrosion inhibitors. Similar trends were observed in the monochloramine reactions with suspended biomass.

483 **Figure 6** is inserted here.

462

463

464

465

466

467

468

469

470

471

472

473

474

475

476

477

478

479

480

481

482

484 485

486

Turning to the cases involving intact biofilms, numerical solutions to Equations [2-6], independently parameterized as described in section 3.4 were used to simulate the dynamics of

disinfectant decay for free chlorine (solid lines in Figure 6a) and for monochloramine (solid lines in Figure 6b), for all three biofilm types. The model underestimated the chlorine consumption within one hour of contact for all three biofilms (t test, p < 0.05). The differences between the simulations and measurements of free chlorine were not statistically significant at all sampling times thereafter in the case of the groundwater biofilms (t test, p > 0.05). However, the model overestimated the free chlorine consumption at 3 and 12 hours of contact and at 3 and 6 hours of contact with phosphate blends and phosphate biofilms, respectively (t test, p < 0.05). Other than the aforementioned contact times for phosphate and phosphate-blends biofilms, the simulation agreed with the measurements (t test, p > 0.05). On the contrary, the model did not agree with the simulations at all sampling time and biofilm growing conditions with monochloramine (t test, p < 0.05). With approximately constant reactive TOC the decay reaction is treated in both free chlorine and monochloramine cases as a first-order reaction with effective rate constant given by the product of the specific rate constant ( $\lambda_o$ ) and biofilm TOC (B). Values for these factors and  $\lambda$  are listed in **Table 1**. Damköhler numbers (reaction rate divided by diffusion rate) are also given in **Table 1** with values generally two orders of magnitude higher for cases involving free chlorine compared to those with monochloramine. This difference is largely attributable to the higher values of the specific decay rate  $\lambda_0$  for free chlorine that are also roughly two orders of magnitude higher than those for monochloramine, while reactive mean biofilm TOC concentration (Table 1) values show only mild differences.

487

488

489

490

491

492

493

494

495

496

497

498

499

500

501

502

503

504

505

506

507

508

509

While differences in overall free chlorine decay patterns among the biofilm types are subtle, the variation of predicted concentrations between biofilm types is larger than the errors between data and simulation in any given case. The predictive simulation of the dynamics in the monochloramine case is much less successful. Simple inspection of the monochloramine decay

in the case of suspended biomass strongly suggested that the reaction was not quasi-first-order as written in Equations [1] and [2] because the trends in disinfectant concentrations are not exponential. Speciation reactions may also complicate the reaction and diffusive transport dynamics (Vikesland et al., 2001). Second, the reaction-diffusion model assumes homogeneous porosity, whereas the pore networks exhibited heterogeneity. It is well known that when reactions are linear (as in the free chlorine case), such small scale heterogeneity does not generally invalidate reactive transport modeling at larger scales under the assumption of effectively homogeneous media; however, this is not demonstrated for nonlinear reactions such as may occur with monochloramine (Murphy and Ginn, 2000, Wood and Whitaker, 1998). Thus, this heterogeneity in pore structure may have a greater impact on monochloramine reactive transport than on free chlorine reactive transport.

#### 4. Conclusions

Biofilm matrix is usually described as a porous material when nutrients, dissolved oxygen, and antimicrobial agents can penetrate the matrix to support or inhibit microbial growth (Lee et al., 2018, Quan et al., 2022). In no flow or slow flow pipes, diffusive transport can dominate the slow-reacting solute transport in biofilms. The reduction in effective diffusion coefficients of chemicals in biofilms suggested that biofilm structure and orientation of water-filled pore space can play an important role in solute transport (Quan et al., 2022). However, due to the complex pore structure and heterogeneity of the biofilm matrix developed under various growing conditions, a single value of effective diffusion coefficient was used in a simplified model system (Davit et al., 2013). The results of this study demonstrated that the porous biofilms developed in phosphate-based corrosion inhibitors lead to a fast depletion of free chlorine in

stagnation. This observation suggested that the effects of pore structure of biofilms on pore-scale reactive-diffusive transport, especially with monochloroamine may need further investigation.

533

534

535

536

537

538

539

540

541

542

543

544

545

546

547

548

549

550

551

552

553

554

555

Simulations of disinfectants in DWDS are widely used in drinking water safety management. The degree to which theoretical reactive-diffusive models can be used to predict the residual disinfectant level in biofilms within pipe networks is an open research question. By relying on a separate set of decay experiments involving suspended biomass from each biofilm, we were able to parameterize a simplified quasi-first-order decay model independently. This model was implemented with a classical diffusion modeling approach with independently determined diffusion parameter values obtained from previous experiments (Chen et al., 1993, Tang and Sandall, 1985). This model was made for a genuinely predictive simulation approach without parameter-fitting. While we found that the classic reactive-diffusive model agreed with the experimental measurements of free chlorine decay with biofilms, the model underestimated the consumption of monochloramine. This underestimation of monochloramine consumption, that our results suggest is primarily due to unincorporated complexities in the reaction network for monochloramine decay within biofilms. Note that monochloramine is recommended over free chlorine to control Legionella pneumophila in building plumbing (National Academies of Sciences and Medicine, 2020). While monochloramine is more effective at inactivating Legionella pneumophila, the underestimation of monochloramine decay could lead to a potential risk of insufficient monochloramine residual in a complex building plumbing with biofilms and stagnation. In a more general context, the modeling results as well as the values of the Damköhler numbers obtained indicate that the diffusion limitation on the decay of disinfectants in the presence of biofilms is significant. However, the simulation of radial diffusion within larger pipe networks incorporating diffusion as described by Equation [2] can be computationally challenging, a first-order or otherwise simplified disinfectant solute exchange processes (Abokifa et al., 2016a) would be worthwhile to improve the model accuracy and alleviate the computational cost.

Due to complex premise plumbing structures, water-saving designs, and human activity, stagnation and slow-flow sections are common in premise plumbing. In this study, we focused on the role of premise plumbing biofilms developed under different chemical conditions on the decay of disinfectants, through both experiments and predictive modeling. Corrosion inhibitors are commonly used to prevent elevated levels of metal leaching from the pipes, especially in aged DWDS. We found that using phosphate-based corrosion inhibitors led to porous biofilms and complete consumption of free chlorine and monochloramine after 24 and 120 hours of stagnation, respectively. After short-term exposure to free chlorine and monochloramine, no significant disturbance in biofilm thickness was observed. This result suggested that short-term disinfectant exposure did not remove biofilm coverage, especially under phosphate-based corrosion inhibition treatment.

## 5. Acknowledgments

- We acknowledge partial support from NSF grants 1855609 and 1855211. We thank Dr. Rosa M.
- 573 Espinosa Marzal and Dr. Mengwei Han (UIUC) for the FTIR scans, Dr. Nicolas Derlon and
- 574 Professor Eberhard Morgenroth (Eawag) for the MATLAB code used for OCT image analysis

#### **6. Authors' Contirbutions**

C.H.: Investigation, validation, methodology, formal analysis, visualization, and writing- original draft except numerical modeling section. T.G.: Methodology, formal analysis, visualization, and writing- original draft, review, and edit on numerical modeling section. G.C.C.: Writing- review

- and edit. F.Z., J.W., and S.A.B.: Methodology, investigation, resources, and visualization on
- 580 OCT image scans. T.H.N.: Conceptualization, supervisation, resources, funding acquisition, and
- writing-original draft, review, and edit.
- **7. Author Disclosure Statement**
- The authors declare that they have no actual or potential competing financial interests.
- **8. Funding Information**
- We acknowledge partial support from NSF grants 1855609 and 1855211.
- 586 9. References
- 587 4500-Cl CHLORINE (RESIDUAL). In: Standard Methods For the Examination of Water and
- Wastewater.
- Abdel-Nour M, Duncan C, Low DE, et al. Biofilms: the stronghold of Legionella pneumophila.
- 590 Int J Mol Sci 2013;14(11):21660-21675; doi: 10.3390/ijms141121660.
- Abokifa AA, Yang YJ, Lo CS, et al. Investigating the role of biofilms in trihalomethane
- formation in water distribution systems with a multicomponent model. Water Research
- 593 2016a;104(Supplement C):208-219; doi: https://doi.org/10.1016/j.watres.2016.08.006.
- Abokifa AA, Yang YJ, Lo CS, et al. Water quality modeling in the dead end sections of drinking
- water distribution networks. Water Research 2016b;89(Supplement C):107-117; doi:
- 596 https://doi.org/10.1016/j.watres.2015.11.025.
- Arnold RB, Rosenfeldt B, Rhoades J, et al. Evolving Utility Practices and Experiences With
- 598 Corrosion Control. Journal American Water Works Association 2020;112(7):26-40; doi:
- 599 10.1002/awwa.1534.
- 600 Bloetscher F, Meeroff DE, Pisani JV, et al. Resolving Problematic Biofilms in Buildings and
- 601 Compounds. Environmental Engineering Science 2010;27(9):767-776; doi:
- 602 10.1089/ees.2009.0422.
- Boccelli DL, Tryby ME, Uber JG, et al. A reactive species model for chlorine decay and THM
- formation under rechlorination conditions. Water Research 2003;37(11):2654-2666; doi:
- 605 https://doi.org/10.1016/S0043-1354(03)00067-8.
- Buse HY, Morris BJ, Struewing IT, et al. Chlorine and Monochloramine Disinfection of
- 607 Legionella pneumophila Colonizing Copper and Polyvinyl Chloride Drinking Water Biofilms.
- Applied and Environmental Microbiology 2019a;85(7):e02956-02918; doi:
- 609 doi:10.1128/AEM.02956-18.
- Buse HY, Morris BJ, Struewing IT, et al. Chlorine and Monochloramine Disinfection of
- 611 Legionella pneumophila Colonizing Copper and Polyvinyl Chloride Drinking Water Biofilms.
- Applied and Environmental Microbiology 2019b;85(7):e02956-02918; doi:
- 613 doi:10.1128/AEM.02956-18.
- 614 Chen CI, Griebe T, Characklis WG. Biocide action of monochloramine on biofilm systems of
- 615 Pseudomonas aeruginosa. Biofouling 1993;7(1):1-17; doi: 10.1080/08927019309386240.

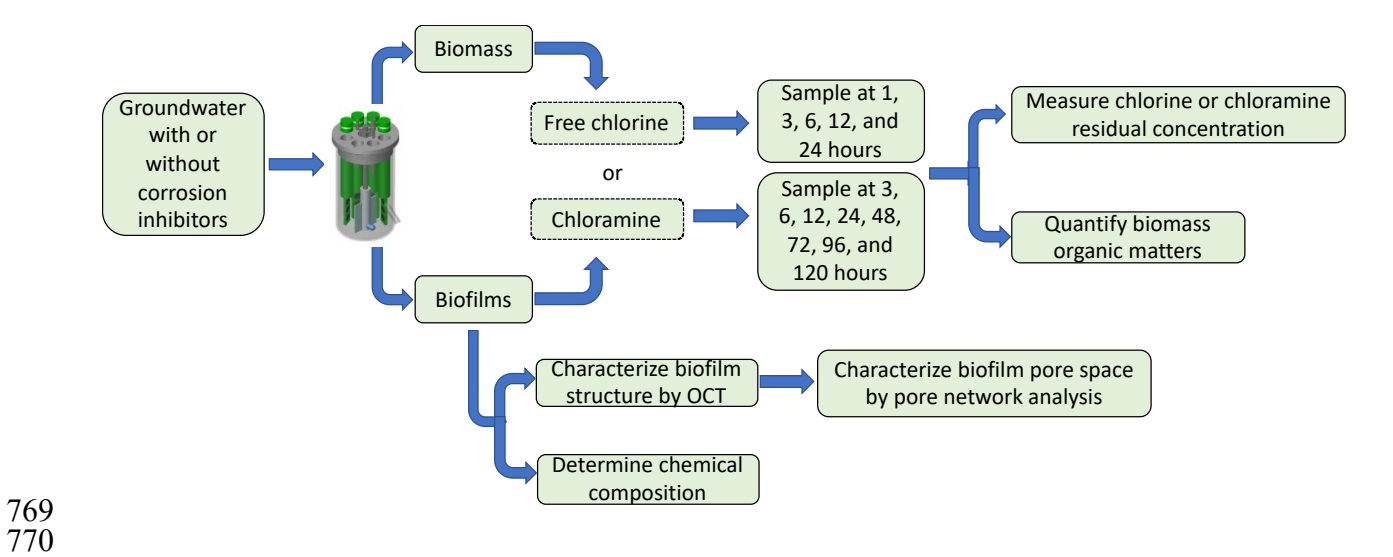
- 616 Cooper IR, Hanlon GW. Resistance of Legionella pneumophila serotype 1 biofilms to chlorine-
- based disinfection. Journal of Hospital Infection 2010;74(2):152-159; doi:
- 618 http://dx.doi.org/10.1016/j.jhin.2009.07.005.
- Davit Y, Byrne H, Osborne J, et al. Hydrodynamic dispersion within porous biofilms. Physical
- 620 Review E 2013;87(1):012718; doi: 10.1103/PhysRevE.87.012718.
- Declerck P. Biofilms: The environmental playground of Legionella pneumophila. Environmental
- 622 Microbiology 2010;12(3):557-566; doi: 10.1111/j.1462-2920.2009.02025.x.
- Declerck P, Behets J, Margineanu A, et al. Replication of Legionella pneumophila in biofilms of
- water distribution pipes. Microbiological Research 2009;164(6):593-603; doi:
- 625 10.1016/j.micres.2007.06.001.
- Derlon N, Peter-Varbanets M, Scheidegger A, et al. Predation influences the structure of biofilm
- developed on ultrafiltration membranes. Water Res 2012;46(10):3323-3333; doi:
- 628 10.1016/j.watres.2012.03.031.
- Douterelo I, Jackson M, Solomon C, et al. Microbial analysis of in situ biofilm formation in
- drinking water distribution systems: implications for monitoring and control of drinking water
- quality. Applied Microbiology and Biotechnology 2016;100(7):3301-3311; doi: 10.1007/s00253-
- 632 015-7155-3.
- Du B, Wang S, Chen G, et al. Nutrient starvation intensifies chlorine disinfection-stressed
- biofilm formation. Chemosphere 2022;295:133827; doi:
- 635 https://doi.org/10.1016/j.chemosphere.2022.133827.
- Fang W, Hu J, Ong SL. Effects of phosphorus on biofilm disinfections in model drinking water
- distribution systems. J Water Health 2010;8(3):446-454; doi: 10.2166/wh.2009.303.
- Fang W, Hu JY, Ong SL. Influence of phosphorus on biofilm formation in model drinking water
- distribution systems. Journal of Applied Microbiology 2009;106(4):1328-1335; doi:
- 640 10.1111/j.1365-2672.2008.04099.x.
- Farhat M, Moletta-Denat M, Frère J, et al. Effects of Disinfection on Legionella spp., Eukarya,
- and Biofilms in a Hot Water System. Applied and Environmental Microbiology
- 643 2012;78(19):6850-6858; doi: 10.1128/aem.00831-12.
- 644 Fish K, Osborn AM, Boxall JB. Biofilm structures (EPS and bacterial communities) in drinking
- water distribution systems are conditioned by hydraulics and influence discolouration. Science of
- 646 The Total Environment 2017;593-594:571-580; doi:
- 647 https://doi.org/10.1016/j.scitotenv.2017.03.176.
- Fish KE, Collins R, Green NH, et al. Characterisation of the physical composition and microbial
- community structure of biofilms within a model full-scale drinking water distribution system.
- 650 PLoS One 2015;10(2):e0115824-e0115824; doi: 10.1371/journal.pone.0115824.
- 651 Goode C, Allen DG. Effect of Calcium on Moving-Bed Biofilm Reactor Biofilms. Water
- 652 Environment Research 2011;83(3):220-232; doi:
- 653 https://doi.org/10.2175/106143010X12780288628255.
- Holman H-YN, Miles R, Hao Z, et al. Real-Time Chemical Imaging of Bacterial Activity in
- 655 Biofilms Using Open-Channel Microfluidics and Synchrotron FTIR Spectromicroscopy.
- 656 Analytical Chemistry 2009;81(20):8564-8570; doi: 10.1021/ac9015424.
- Huang C, Shen Y, Smith RL, et al. Effect of disinfectant residuals on infection risks from
- 658 Legionella pneumophila released by biofilms grown under simulated premise plumbing
- conditions. Environment International 2020a;137:105561; doi:
- 660 https://doi.org/10.1016/j.envint.2020.105561.

- Huang C, Sun PP, Won J, et al. Effect of Nonphosphorus Corrosion Inhibitors on Biofilm Pore
- Structure and Mechanical Properties. Environmental science & technology 2020b;54(22):14716-
- 663 14724; doi: 10.1021/acs.est.0c04645.
- Kogo A, Payne SJ, Andrews RC. Impact of Corrosion Control on Biofilm Development in
- 665 Simulated Partial Lead Service Line Replacements. Environmental Engineering Science
- 666 2017;34(10):711-720; doi: 10.1089/ees.2016.0507.
- Lautenschlager K, Boon N, Wang Y, et al. Overnight stagnation of drinking water in household
- taps induces microbial growth and changes in community composition. Water Research
- 669 2010;44(17):4868-4877; doi: <a href="https://doi.org/10.1016/j.watres.2010.07.032">https://doi.org/10.1016/j.watres.2010.07.032</a>.
- 670 Lee WH, Pressman JG, Wahman DG. Three-Dimensional Free Chlorine and Monochloramine
- Biofilm Penetration: Correlating Penetration with Biofilm Activity and Viability. Environmental
- 672 science & technology 2018;52(4):1889-1898; doi: 10.1021/acs.est.7b05215.
- Lee WH, Wahman DG, Bishop PL, et al. Free Chlorine and Monochloramine Application to
- Nitrifying Biofilm: Comparison of Biofilm Penetration, Activity, and Viability. Environmental
- 675 science & technology 2011;45(4):1412-1419; doi: 10.1021/es1035305.
- 676 Lemus Pérez MF, Rodríguez Susa M. Exopolymeric substances from drinking water biofilms:
- 677 Dynamics of production and relation with disinfection by products. Water Research
- 678 2017;116(Supplement C):304-315; doi: https://doi.org/10.1016/j.watres.2017.03.036.
- 679 Ley CJ, Proctor CR, Singh G, et al. Drinking water microbiology in a water-efficient building:
- stagnation, seasonality, and physicochemical effects on opportunistic pathogen and total bacteria
- proliferation. Environmental Science: Water Research & Technology 2020;6(10):2902-2913;
- 682 doi: 10.1039/D0EW00334D.
- 683 Li RA, McDonald JA, Sathasivan A, et al. Disinfectant residual stability leading to disinfectant
- decay and by-product formation in drinking water distribution systems: A systematic review.
- Water Research 2019;153:335-348; doi: https://doi.org/10.1016/j.watres.2019.01.020.
- 686 Ling F, Whitaker R, LeChevallier MW, et al. Drinking water microbiome assembly induced by
- 687 water stagnation. The ISME Journal 2018; doi: 10.1038/s41396-018-0101-5.
- 688 Liu L, Hu Q, Le Y, et al. Chlorination-mediated EPS excretion shapes early-stage biofilm
- 689 formation in drinking water systems. Process Biochemistry 2017;55:41-48; doi:
- 690 https://doi.org/10.1016/j.procbio.2016.12.029.
- 691 Liu S, Gunawan C, Barraud N, et al. Understanding, Monitoring, and Controlling Biofilm
- 692 Growth in Drinking Water Distribution Systems. Environmental science & technology
- 693 2016;50(17):8954-8976; doi: 10.1021/acs.est.6b00835.
- McNeill LS, Edwards M. Phosphate inhibitor use at US utilities. Journal (American Water
- 695 Works Association) 2002;94(7):57-63.
- Melo LF. Biofilm physical structure, internal diffusivity and tortuosity. Water Science and
- 697 Technology 2005;52(7):77-84; doi: 10.2166/wst.2005.0184.
- Monteiro L, Figueiredo D, Dias S, et al. Modeling of Chlorine Decay in Drinking Water Supply
- 699 Systems Using EPANET MSX. Procedia Engineering 2014;70:1192-1200; doi:
- 700 https://doi.org/10.1016/j.proeng.2014.02.132.
- 701 Murphy EM, Ginn TR. Modeling microbial processes in porous media. Hydrogeology Journal
- 702 2000;8(1):142-158; doi: 10.1007/s100409900043.
- National Academies of Sciences E, Medicine. Management of Legionella in Water Systems. The
- National Academies Press: Washington, DC; 2020.

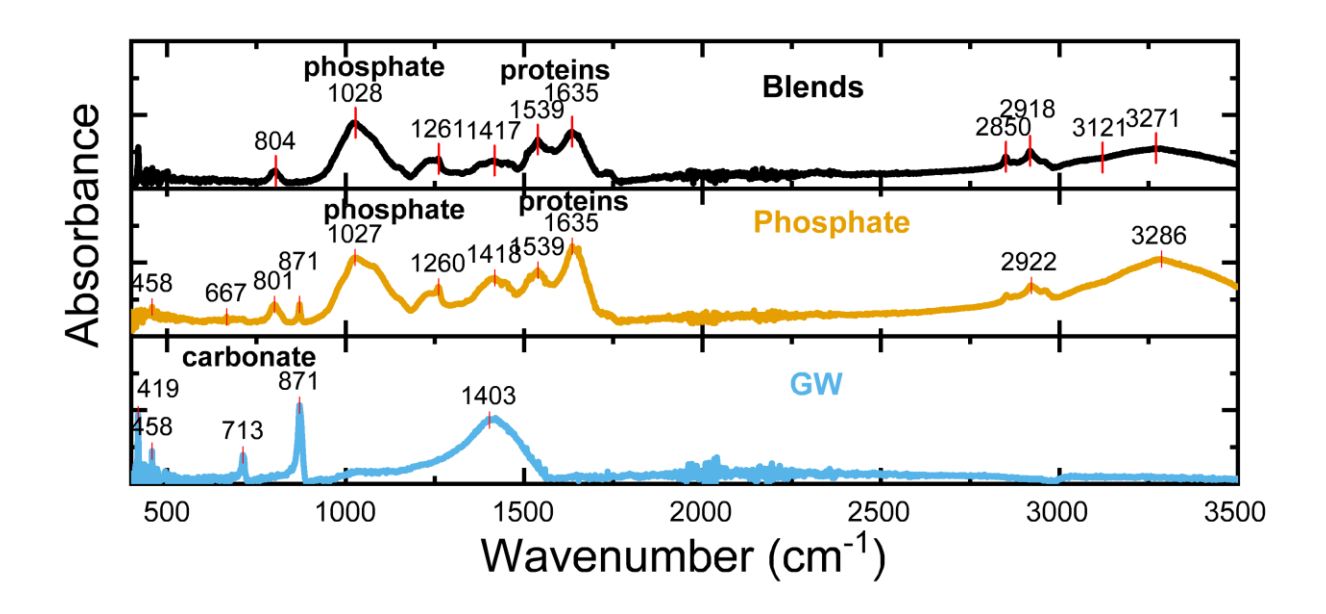
- Pousti M, Joly M, Roberge P, et al. Linear Scanning ATR-FTIR for Chemical Mapping and
- 706 High-Throughput Studies of *Pseudomonas sp.* Biofilms in Microfluidic Channels. Analytical
- 707 Chemistry 2018;90(24):14475-14483; doi: 10.1021/acs.analchem.8b04279.
- 708 Prest EI, Hammes F, van Loosdrecht MCM, et al. Biological Stability of Drinking Water:
- 709 Controlling Factors, Methods, and Challenges. Frontiers in Microbiology 2016;7(45); doi:
- 710 10.3389/fmicb.2016.00045.
- Quan K, Hou J, Zhang Z, et al. Water in bacterial biofilms: pores and channels, storage and
- 712 transport functions. Critical Reviews in Microbiology 2022;48(3):283-302; doi:
- 713 10.1080/1040841X.2021.1962802.
- Quilès F, Humbert F, Delille A. Analysis of changes in attenuated total reflection FTIR
- fingerprints of *Pseudomonas* fluorescens from planktonic state to nascent biofilm state.
- 716 Spectrochimica Acta Part A: Molecular and Biomolecular Spectroscopy 2010;75(2):610-616;
- 717 doi: https://doi.org/10.1016/j.saa.2009.11.026.
- Rennecker JL, Kim J-H, Corona-Vasquez B, et al. Role of Disinfectant Concentration and pH in
- the Inactivation Kinetics of Cryptosporidium parvum Oocysts with Ozone and Monochloramine.
- 720 Environmental science & technology 2001;35(13):2752-2757; doi: 10.1021/es010526z.
- Schindelin J, Arganda-Carreras I, Frise E, et al. Fiji: an open-source platform for biological-
- 722 image analysis. Nature Methods 2012;9(7):676-682; doi: 10.1038/nmeth.2019.
- 723 Schmitt J, Flemming H-C. FTIR-spectroscopy in microbial and material analysis. International
- Biodeterioration & Biodegradation 1998;41(1):1-11; doi: https://doi.org/10.1016/S0964-
- 725 8305(98)80002-4.
- Shen Y, Huang PC, Huang C, et al. Effect of divalent ions and a polyphosphate on composition,
- structure, and stiffness of simulated drinking water biofilms. npj Biofilms and Microbiomes
- 728 2018;4(1):15; doi: 10.1038/s41522-018-0058-1.
- Shen Y, Monroy GL, Derlon N, et al. Role of Biofilm Roughness and Hydrodynamic Conditions
- 730 in Legionella pneumophila Adhesion to and Detachment from Simulated Drinking Water
- 731 Biofilms. Environmental science & technology 2015;49(7):4274-4282; doi: 10.1021/es505842v.
- 732 Tang A, Sandall OC. Diffusion coefficient of chlorine in water at 25-60.degree.C. Journal of
- 733 Chemical & Engineering Data 1985;30(2):189-191; doi: 10.1021/je00040a017.
- 734 Tolofari DL, Bartrand T, Masters SV, et al. Influence of Hot Water Temperature and Use
- 735 Patterns on Microbial Water Quality in Building Plumbing Systems. Environmental Engineering
- 736 Science 2021;39(4):309-319; doi: 10.1089/ees.2021.0272.
- 737 Tugarova AV, Scheludko AV, Dyatlova YA, et al. FTIR spectroscopic study of biofilms formed
- by the rhizobacterium Azospirillum brasilense Sp245 and its mutant Azospirillum brasilense
- 739 Sp245.1610. Journal of Molecular Structure 2017;1140:142-147; doi:
- 740 https://doi.org/10.1016/j.molstruc.2016.12.063.
- 741 USEPA. Optimal Corrosion Control Treatment Evaluation Technical Recommendations for
- Primacy Agencies and Public Water Systems. In: ((4606M) OoW ed.) 2016.
- Vikesland PJ, Ozekin K, Valentine RL. Monochloramine decay in model and distribution system
- 744 waters. Water Res 2001;35(7):1766-1776; doi: 10.1016/s0043-1354(00)00406-1.
- Wang H, Masters S, Hong Y, et al. Effect of Disinfectant, Water Age, and Pipe Material on
- Occurrence and Persistence of Legionella, mycobacteria, Pseudomonas aeruginosa, and Two
- 747 Amoebas. Environmental science & technology 2012;46(21):11566-11574; doi:
- 748 10.1021/es303212a.

- Wang J-J, Liu X, Ng TW, et al. Disinfection byproduct formation from chlorination of pure
- bacterial cells and pipeline biofilms. Water Research 2013a;47(8):2701-2709; doi:
- 751 https://doi.org/10.1016/j.watres.2013.02.038.
- Wang Z, Choi O, Seo Y. Relative contribution of biomolecules in bacterial extracellular
- 753 polymeric substances to disinfection byproduct formation. Environmental science & technology
- 754 2013b;47(17):9764-9773; doi: 10.1021/es402067g.
- Wood BD, Whitaker S. Diffusion and reaction in biofilms. Chemical Engineering Science
- 756 1998;53(3):397-425; doi: https://doi.org/10.1016/S0009-2509(97)00319-9.
- 757 Xue Z, Seo Y. Impact of Chlorine Disinfection on Redistribution of Cell Clusters from Biofilms.
- 758 Environmental science & technology 2013;47(3):1365-1372; doi: 10.1021/es304113e.
- 759 Zhao Y, Yang YJ, Shao Y, et al. The dependence of chlorine decay and DBP formation kinetics
- on pipe flow properties in drinking water distribution. Water Research 2018; doi:
- 761 https://doi.org/10.1016/j.watres.2018.04.048.

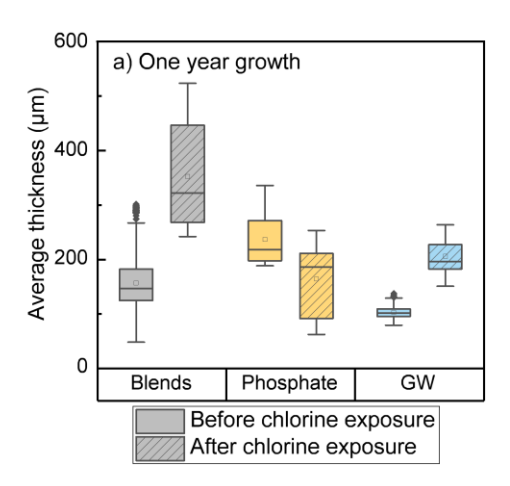
- Zheng M, He C, He Q. Fate of free chlorine in drinking water during distribution in premise
- 763 plumbing. Ecotoxicology 2015;24(10):2151-2155; doi: 10.1007/s10646-015-1544-3.
- 764 Zhu N, Mapili K, Majeed H, et al. Sediment and biofilm affect disinfectant decay rates during
- long-term operation of simulated reclaimed water distribution systems. Environmental Science:
- 766 Water Research & Technology 2020;6(6):1615-1626; doi: 10.1039/C9EW00978G.

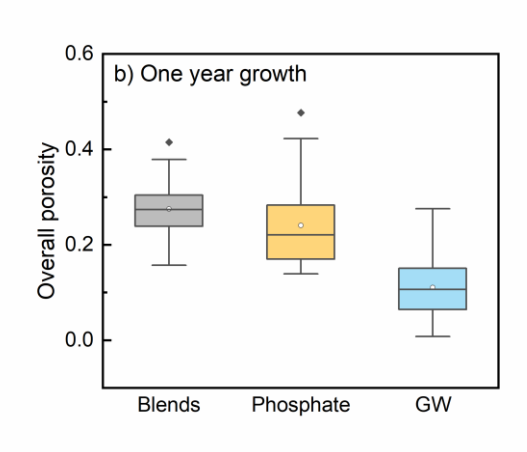


**Figure 1**. Flow diagram for experiments to characterize biofilm structure and disinfectant consumption. The reaction times of suspended biomass were 5, 15, 30, 150 min with free chlorine and 3, 6, 12, 24, and 48 hours with monochloramine.

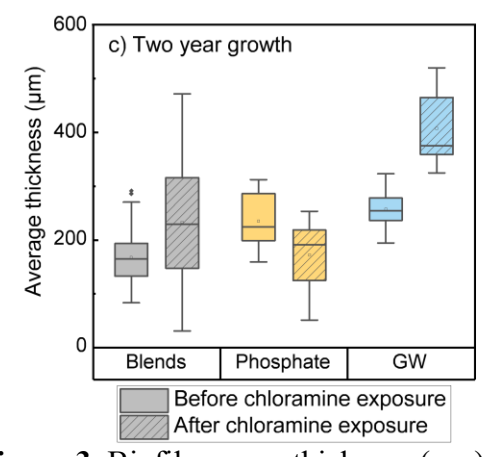


**Figure 2.** IR spectrums of two-year biofilms developed in groundwater (blue) and groundwater amended with phosphate (yellow), or phosphate blends (black).









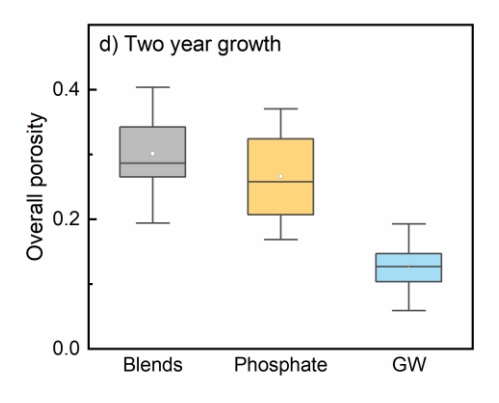


**Figure 3**. Biofilm mean thickness (a, c) and overall porosities (b, d) in phosphate blends (grey), phosphate (yellow), and groundwater (blue) biofilms in a and b (one-year-old biofilms) and c and d (two-year-old biofilms). Solid lines indicate medians and boxes indicate the 25-75 percentiles of the distributions. Open circles indicate means and solid circles indicate outliers.

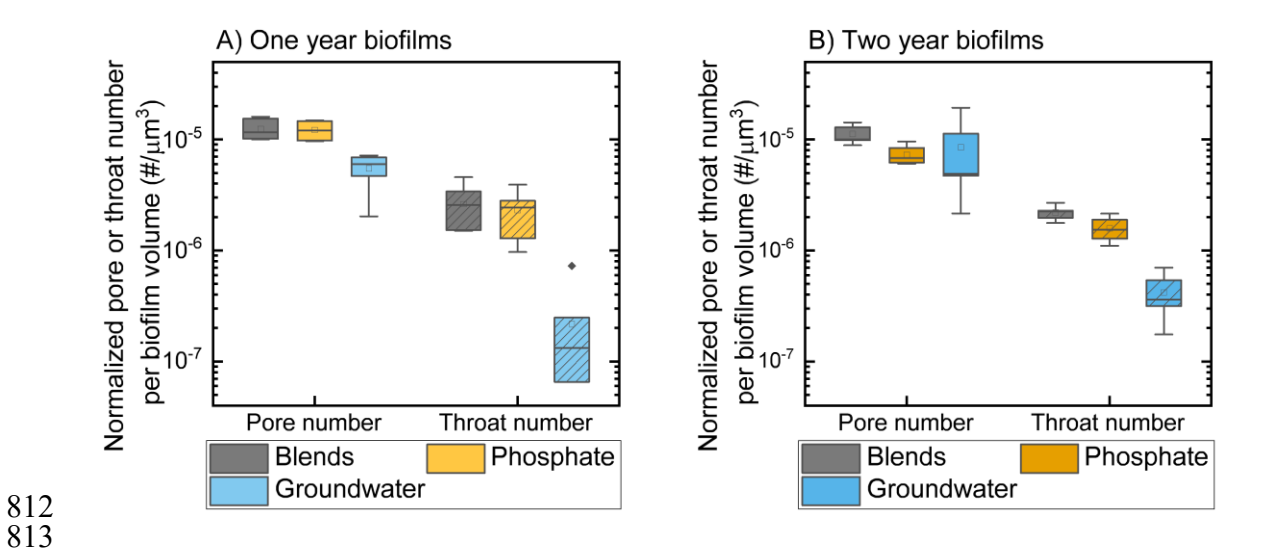


**Figure 4.** Pore (solid) and throat (dashed) number normalized by biofilm volume after A) one-year and B) two-year growth. The lines indicate medians, and the boxes mark the 25-75 quantiles. Open circles represent means.

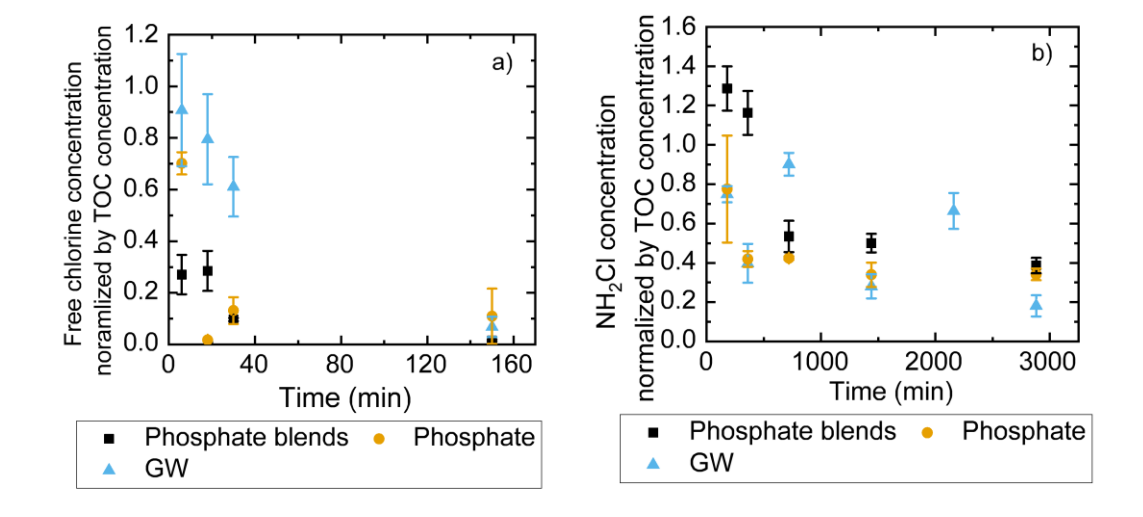


**Figure 5**. The experimentally measured free chlorine a) or chloramine (b) concentrations were normalized by the TOC concentration ([mg/L as Cl<sub>2</sub>] /[mg/L as C]) obtained from the phosphate blends (black square), phosphate (yellow circle), and groundwater (blue triangle) biomass suspensions.

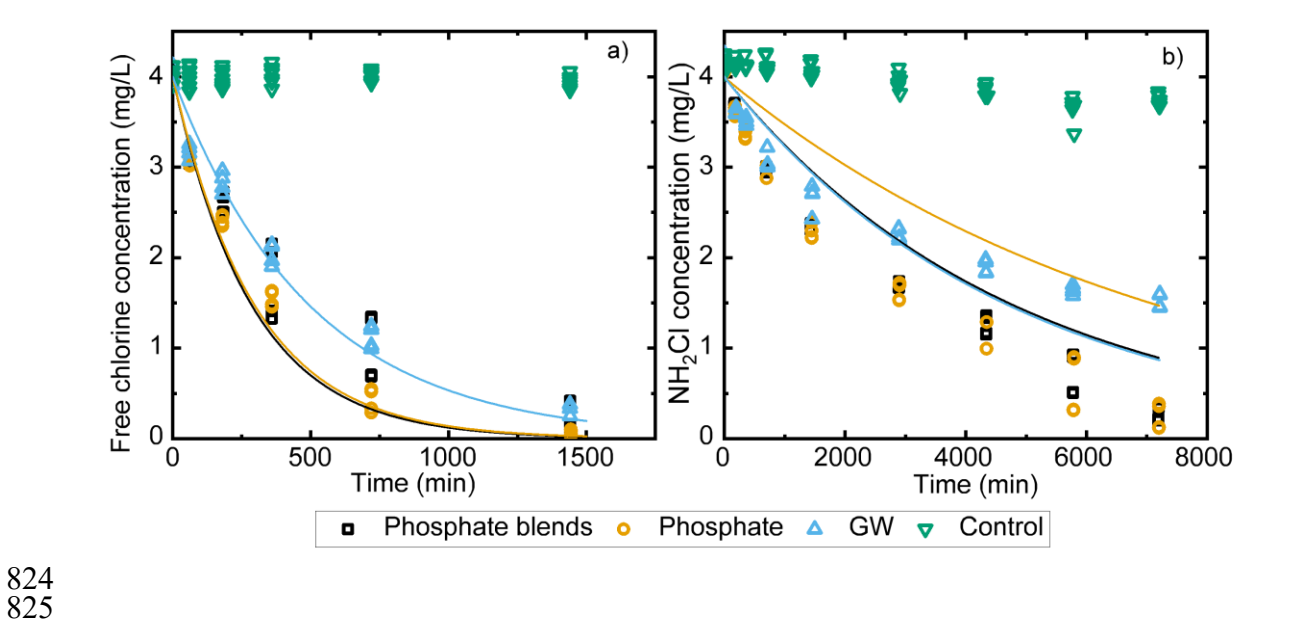


**Figure 6**. Free chlorine (a) and monochloramine (b) decay in contact with phosphate blends (black square), phosphate (yellow circle), and groundwater biofilms (blue triangle) after stagnation. Light green scatters represent the disinfectant decay in the control buffer. Solid lines are the simulated free chlorine or chloramine decay in contact with the three biofilms by solution of Equations [2-6] as described in Section 2.5.